International Journal of Innovative Technology and Exploring Engineering (IJITEE)
ISSN: 2278-3075 (Online), Volume-9 Issue-4, February 2020

Thermal Performance Improvement of a Fin-Arrayed Horizontal Heat Sink Corroborating Optimal Orientation Angle

Pabitra Kumar Mandal, Sayantan Sengupta, Subhas Chandra Rana, Dipankar Bhanja

Abstract*: *The present study deals with a simple but effective technique for improving the forced convective cooling of a horizontal heat sink with vertical pin-fin-array.The pin fins are embedded in a staggered arrangement on thebase-plate of the horizontal sink. Air, while passing through the fin-array, convects the heat conducted from the solid base-plate to the fins' surface. The objective of this paper is to examine the role of the orientation angle (β) on the performance of the heat sink. β is varied from 0° to 360° by rotating the horizontal sink about a vertical axis passing through the center of the sink. A detailed CFD (computational fluid dynamics) study is coordinated over a wide range of inflow Reynolds number (Re) to explore the possibility for obtaining an optimum orientation angle (β) for which Nusselt number (Nu) would be the maximum. Results indicate that optimum angle hovers around $\beta = 120^\circ$ regardless of the values of Re.

Keywords* : *Heat sink, performance, staggered fins, CFD, Orientation angle.

I. INTRODUCTION

In heat exchange devices, extended surfaces or fins are often used in order to increase the heat transfer between the original surface (either heated or cooled) and the fluid surrounding it. The fins are indispensable for evaporator coils in room-air-conditioners, heat sinks of electronic appliances, in the design of cooling devices in automobiles and aircrafts, etc. In practice, different types of fins e.g. straight fin, pin fin and annular fin, etc.

Revised Manuscript Received on February 28, 2020.
***** Correspondence Author
Pabitra Kumar Mandal*, Department of Mechanical Engineering, Dr. B.C. Roy Engineering College, Durgapur, 713206 (W.B.), India Department of Mechanical Engineering, National Institute of Technology, Durgapur, 713209 (W.B.), India pabitra.mandal@bcrec.ac.in
Sayantan Sengupta,Department of Mechanical Engineering, National Institute of Technology, Durgapur, 713209 (W.B.), India sayantanjgec@gmail.com
Subhas Chandra Rana, Department of Mechanical Engineering, National Institute of Technology, Durgapur, 713209 (W.B.), India subhas.rana@me.nitdgp.ac.in
Dipankar Bhanja, Department of Mechanical Engineering, National Institute of Technology, Silchar, 788010 (Assam), India dipankar.bhanja@gmail.com

are used depending on the specific application areas. Usually, a pin fin is a solid cylinder connected perpendicular to a wall, and a cross-flow is performed to transfer heat from the surfaces of the cylinder to the passing fluid. One advantage of using pin fin over the other shaped fins is its manufacturing simplicity. Most of the time, pin fins are arranged in arrays, either in-line or staggered with respect to the direction of flow. Sparrow et al. (1980) made a detailed study comparing the performances of in-line and staggered arrays, and came to the conclusion that the fully developed convective heat transfer coefficients for a staggered array are greater than those for an in-line array, but the pressure drop is also greater. According to them, for fixed values of pumping power and heat transfer area, a staggered array transfers less heat than an in-line array. However, when heat load and mass flow rate are fixed, the staggered array demands a smaller heat transfer surface as compared to the in-line array. The present paper deals with a situation in which heat load and mass flow rate are fixed; hence, we would focus our attention on a staggered fin array. A few other advantages of staggered arrangement over inline arrangement are demonstrated in Salviano et al. (2016). Literature shows that studies with fins have been performed with and without tip insulation. Li (1983), Sonn and Bar-cohen (1981), and many others (Haley and Westwater 1966, Razani and Zahoor, 1991,Yeh and Liaw, 1993) considered insulated tip. On the other hand, Yeh (1997) investigated the effects of heat transfer from the fin tip. Yeh concluded that at a specified heat transfer mode, the optimum aspect ratio (height/diameter) of a fin is the highest for a fin with an insulated tip and reduces with an increase in the rate of heat transfer from the tip. We, however, restricted our study for the case of insulated tips. Various attempts had been made in the past to improve the performance of a single pin fin. Previous researchers determined the optimum height(*H*) and diameter (*D*) of a single pin fin [Eckert and Drake (1972),Zukauskas (1972), Sonn and Bar-cohen (1981), Li (1983),and Yeh (1997)].Having determined the optimum diameter and length of a pin fin, the researchers attempted various alterations on conventional pin fins for achieving a further improvement in its performance. Among these, porous pin fins [Seyf and Layeghi (2010), Bhanja et al. (2013), Vahabzadehet al. (2015)], perforated pin fins [SahinandDemir (2008), Maji et al. (2017), Chin et al. (2013), Al-Damook et al.(2015, 2016)],excavated pin fins [Yeh and Liaw (1993), Liaw et al. (2005), Elshafei (2010),Lin et al. (2014)] are worth mentioning. According to literatures [Bhanja et al. (2013)], porousfins are good passive means to provide high heat transfer rate for small electronic parts in a light-weight package.

Most of the previous papers indicate that porous fins are good in natural convective flows. We, however, deal with forced convective flow. Reduction of fin's weight and greater heat transfer rate are the benefits of perforated fins. However, in external applications where deposition of dust particles is a serious issue, the perforations may be choked, resulting in the gradual decay of the performance of the fin array. Excavated fins provide greater contact surface-area between the fin's material and the fluid. One of the disadvantages of the excavated fins is its low strength. In case of modern electronic appliances, the size of the fins is often so small that perforated and excavated fins may not produce the necessary strength or durability. The thermo-fluid dynamics of a pin-fin array is much more complex than a single pin-fin, primarily because of the presence of three additional characteristics dimensions viz., L_{Row} , L_{Pitch} and L_{Offset} .These three determine the positioning of fins in the array. Figure 1 shows a schematic of the physical configuration. The square shaped horizontal base-plate of the heat sink further invokes two additional physical parameters, viz. length (*L)* and thickness (*h*) of the plate. Recently, Chin et al. (2013) performed experiments and conducted computational studies with a horizontal staggered pin-fin array. In their study, *L*=100mm and *h*=3mm, *H*=50mm, *D*=8mm, $L_{Row} = 25\ \text{mm}$, $L_{Pitch} = 25\ \text{mm}$ and $L_{Offset} = 12.5\ \text{mm}$ .In the present CFD study, all physical dimensions of the heat sink are the same as in Chin et al. (2013). A few methods employed by previous researchers for performance enhancement of a horizontal fin-arrayed heat sink are shape-modification of individual fin (e.g. perforated and excavated) or utilization of improved fins' materials (e.g. porous).[A few other interesting researches with pin fin arrayed heat sink are found in Yu et al. (2005), Yang et al. (2016) and Zhao et al. (2016).] In this paper, we have introduced a new method to regulate the performance of a horizontal fin-arrayed heat sink. In this method, the orientation angle (β) of the horizontal sink is varied. The orientation angle is varied by rotating the horizontal sink about a vertical axis passing through the center of the sink (see Figure 2). A detailed CFD (computational fluid dynamics) study is performed with an objective to examine the role of the orientation angle (β) on the heat transfer characteristics and power requirement of the heat sink. To the best of our knowledge, the present study is the first of its kind. Interesting findings and necessary analyses have been provided in Section 3.

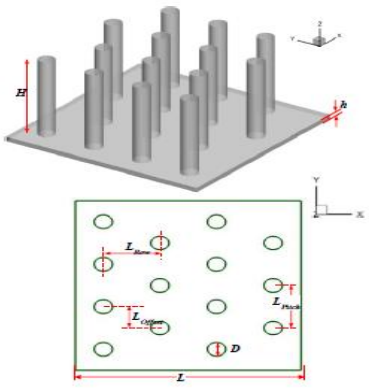

Figure 1 Schematic diagram of the heat sink with staggered fin array

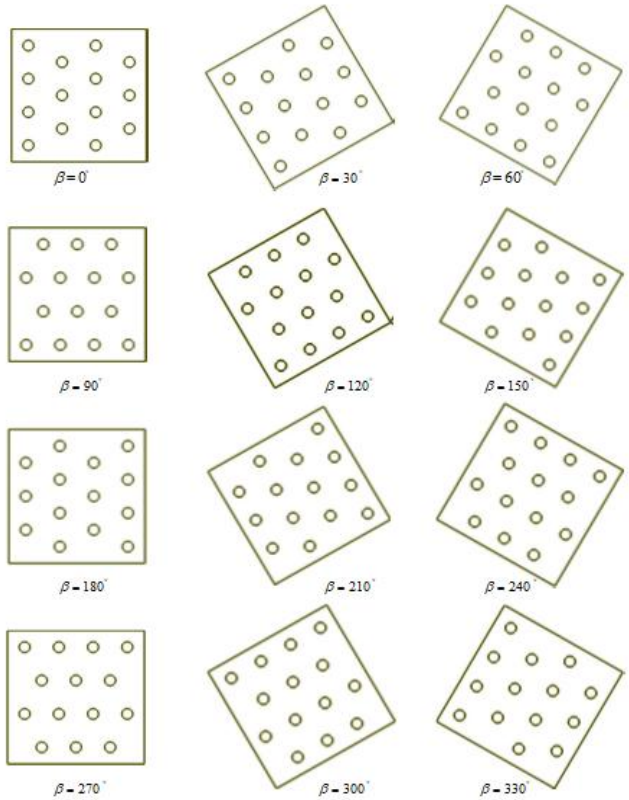

Figure 2 Various orientations of the horizontal fin-arrayed heat sink about the z-axis, perpendicular to the plane of this paper (anti-clockwise rotation has been considered).

II. COMPUTATIONAL METHOD

Figure 3 shows the present computational domain comprising a rectangular channel and a solid fin-arrayed heat sink. The heat sink consists of a square base plate and an array of solid pin fins. It is mounted inside the rectangular channel. The physical dimensions of the square base plate are as follows: length L =100mm and thickness *h*=3mm.The length (L_c), width (W_c), and height (H_c) of the rectangular channel are 1050mm, 100√2mm and 50mm, respectively.

The hydraulic diameter d_h (equation1) of the rectangular channel is 0.07389mm.

$$d_h = 4(W_c H_c)/2(W_c + H_c) \quad (1)$$

Air enters the rectangular channel through the face ABCD; it absorbs heat from the heated horizontal plate and fin array; and, then leaves the channel through the face EFGH. The *x*-distance between the face ABCD and center of the base plate is 800mm; and, the *x*-distance between the face EFGH and center of the base plate is 250mm. These large *x*-distances are set so that the boundary conditions prescribed at the inlet and outlet would not affect the fluid dynamics immediately before and after the heat sink. The y-distance between a side wall and center of the base plate is $100/\sqrt{2}$mm.

Three-dimensional CFD simulations have been performed to analyze the forced convective flow through staggered pin fin arrays. Navier-Stokes equations [Burmeister (1993)] for steady, incompressible flow are as follows:
Continuity equation:

$$\nabla \cdot (\rho \vec{v}) = 0 \quad (2)$$

Momentum equation:

$$\rho \vec{v} \cdot \nabla \vec{v} = \mu \nabla^2 \vec{v} - \nabla p \quad (3)$$

Energy equation:

$$\rho c_p \nabla \cdot (\vec{v} T) = \nabla \cdot (K \nabla T) \quad (4)$$

Realizable $k-\varepsilon$ model with standard wall function is used for simulating the turbulence in the flow field used in the present problem. The transport equations corresponding to turbulent kinetic energy (k) and turbulent dissipation (ε) in Realizable $k-\varepsilon$ model along with the Reynolds Average Navier-Stokes (RANS) and energy equation are given below.

$$\frac{\partial}{\partial x_j}(\rho u_j) = 0 \quad (4a)$$

$$\rho \frac{Du_i}{Dt} = -\frac{\partial P}{\partial x_j} + \frac{\partial}{\partial x_i}\left[\mu\left(\frac{\partial u_i}{\partial xi} + \frac{\partial u_j}{\partial x_i} - \frac{2}{3}\delta_{ij}\frac{\partial u_i}{\partial x_i}\right)\right] + \frac{\partial}{\partial x_i}\left(\overline{-\rho u_i' u_j'}\right)$$

$$(4b)\ \frac{\partial}{\partial x_j}(\rho k u_j) = \frac{\partial}{\partial x_j}\left[\left(\mu + \frac{\mu_t}{\sigma_k}\right)\frac{\partial k}{\partial x_j}\right] + G_k + G_b - \rho_\varepsilon + Y_M$$

$$(5)\ \frac{\partial}{\partial x_j}(\rho \varepsilon u_j) = \frac{\partial}{\partial x_j}\left[\left(\mu + \frac{\mu_t}{\sigma_\varepsilon}\right)\frac{\partial \varepsilon}{\partial x_j}\right] - \rho C_2 \frac{\varepsilon^2}{k + \sqrt{\nu\varepsilon}} + C_{1\varepsilon}\frac{\varepsilon}{k} C_{3\varepsilon} G_b \quad (6)$$

The Energy equation for present problem is

$$\frac{DT}{Dt} = \frac{\partial}{\partial x_i}\left[(\alpha + \alpha_t)\frac{\partial T}{\partial x_i}\right] \quad (7)$$

The additional terms $\overline{-\rho u_i' u_j'}$ in the momentum equation (4b) are termed as the Reynolds stresses. These stresses are modeled by Boussinesq hypothesis which is given below:

$$\overline{-\rho u_i' u_j'} = \mu_t\left(\frac{\partial u_i}{\partial x_j} + \frac{\partial u_j}{\partial x_i}\right) - \frac{2}{3}\left(\rho k + \mu_t \frac{\partial u_i}{\partial x_i}\right)\delta_{ij} \quad (8)$$

$$\mu_t = \rho C_\mu \frac{k^2}{\varepsilon} \quad (9)$$

where, μ_t is eddy viscosity or turbulent viscosity, k is the turbulent kinetic energy, ε is the turbulent dissipation rate $\alpha_t = \frac{\mu_t}{\rho \sigma_t}$ is turbulent diffusivity and σ_t is turbulent Prandtl number. In standard $k-\varepsilon$ model $C_\mu = 0.09$ but in Realizable $k-\varepsilon$ model C_μ is variable which provides improved predictions.

In equations (4a)-(8), G_k is the generation of turbulence kinetic energy due to the mean velocity gradients, G_b represents the generation of turbulence kinetic energy due to buoyancy, Y_M is the contribution of the fluctuating dilatation in compressible turbulence to the overall dissipation rate, σ_k and σ_ε are the turbulent Prandtl numbers for k and ε, respectively.

In Realizable $k-\varepsilon$ model, the default values for the constants are as follows: $\sigma_k = \sigma_t = 1.0$, $\sigma_\varepsilon = 1.2$, $C_{1\varepsilon} = 1.44$, and $C_2 = 1.9$.

A pressure-based, steady solver of commercially available finite volume software Fluent 16.0 [Fluent 16.0 User's Guide] is employed to solve the set of equations (2)-(6). The coupling between the pressure and velocity is done by SIMPLE algorithm [Patankar(1980)]. The spatial discretization for the convective terms is carried out by using second order upwind scheme. The pressure terms are interpolated by using a second order scheme available in Fluent 16.0. Least square cell-based algorithm is utilized to determine the gradients in the conservation equations. The under-relaxation factors for pressure, density, body force, momentum, turbulent kinetic energy, turbulent dissipation rate, turbulent viscosity and energy are 0.3, 1, 1, 0.7, 0.8, 0.8, 1 and 1, respectively. The combination provides a stable but quicker progress of convergence.

Equations (2)-(6) are solved for the following boundary conditions. At the inlet face (ABCD in Figure 3), the velocity, temperature and turbulent intensity of inflow are specified. We have used T_{in} = 300 K and k_{in} = 10%. Simulations are performed over a wide range of Reynolds number ($8500 < Re < 36000$), where $\mathrm{Re} = \rho \bar{V} d_h / \mu$. The Reynolds number is varied by changing v_x (x- velocity) only. The range of Reynolds number corresponds to $2\ \mathrm{m/s} < v_x < 8\ \mathrm{m/s}$ air velocity used in many heat sink applications. At the inlet, $v_y = v_z = 0$. The exit plane EFGH is modeled by the 'pressure outlet' condition [Fluent 16.0 User's Guide]. This condition sets a zero gauge pressure on the exit plane. Wall boundary condition is imposed on all other faces of the rectangular channel. These walls are thermally insulated. Wall boundary condition is also imposed on all faces of the solid test rig. No slip condition is specified at all wall boundaries. The bottom surface of the base plate is subjected to a constant heat flux, q_w (the value being 5903 $\mathrm{W/m^2}$ i.e. the same as used by Chin et al. in their experiments), the side surfaces of the base plate are thermally insulated. 'Coupled condition' [Fluent 16.0 User's Guide] is employed at the top surface of the base plate and at the surfaces of the fins exposed to fluid flow.

The material for the base plate and the fin-array is an aluminum alloy. The density (ρ), thermal conductivity (K) and c_p values of the aluminum alloy are 2719 $\mathrm{kg/m^3}$, 167 $\mathrm{W/m\,K}$ and 871 $\mathrm{J/kg\,K}$, respectively. The working fluid is air. The density of air is modeled by incompressible ideal gas; and, its viscosity (μ), thermal conductivity (K) and c_p values are specified as 1.7894×10^{-5} $\mathrm{kg/m\,s}$, 0.0242 $\mathrm{W/m\,K}$ and 1006.43 $\mathrm{J/kg\,K}$, respectively.

The accuracy of the CFD results has been ensured by grid independence test and convergence criterion test. A maximum scaled residual [Fluent 16.0 User's Guide] of 10^{-6} is used as the convergence criterion for the present study. Grid independence test has been performed in order to determine the optimum number of computational cells necessary for obtaining reasonably accurate results. We have used triangular, unstructured grids. A few pertinent details are given in Table 1. For the sake of validating our CFD method, we compare our CFD solutions with recently published experimental data given in Chin et al. (2013). Figure 4 shows that our CFD solutions are in good agreement with the experimental data given in Chin et al. (2013). In this regard, it should be noted that as compared to Chin et al., we used a slightly larger hydraulic diameter to accommodate the maximum possible width of the heat sink (i.e. the diagonal length of the base plate, 100√2mm) inside the rectangular channel.

Table 1 Grid independence test ($q_w = 5903$ $\mathrm{W/m^2}$, $T_{in} = 300$ K, $\beta = 0^{\circ}$ and air as working fluid)

Re	Grid distribution	No. of Cells	Area averaged static pressure at the inlet (Pa)	Area averaged temperature of the heated surface (K)
9380	Coarse	1221734	3.18	355.18
	Normal	2747871	3.40	348.41
	Fine	5115298	3.45	348.16
35860	Coarse	1221734	33.33	333.68
	Normal	2747871	30.81	331.52
	Fine	5115298	30.50	331.27

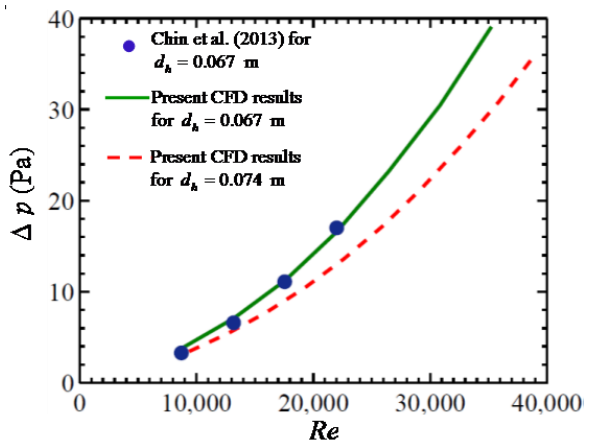

(a)

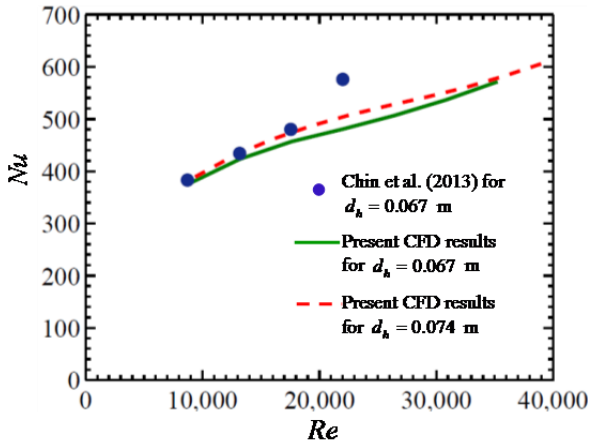

(b)

Figure 4Validation of the present CFD results (a) Pressure drop (Δp) versus Reynolds number; (b) Nusselt number (Nu) versus Reynolds number (Re)

III. RESULTS AND DISCUSSION

At the inlet plane ABCD (Figure 3), the velocity vectors have only one non-zero component, i.e. v_x . In the downstream, v_y and v_z are developed inside the boundary layers appearing due to the no slip condition imposed at the channel walls. However, in this region, the magnitudes of v_y and v_z are small in the bulk flow. The fluid dynamics is very complex adjacent to the heat-sink due to the presence of solid fin array. An attempt is made below to describe some subtleties of this complex flow. Flow past a circular cylinder is routinely included in all text books of fluid mechanics. Here, we are dealing with an array of cylinders instead of a single cylinder. Consider the first row. The dominating (or, major) velocity component immediately before this row is v_x . Having intercepted by the row, v_y would increase substantially, and v_y would be of the order of v_x .Figure 5 is drawn to show the pattern of streamlines and contours of flow variables correspond to $\beta = 0$, $q_w = 5903$ $\mathrm{W/m^2}$, $T_{in} = 300$ K, and $\mathrm{Re} = 19290$. Figure 5ashows the contours of *x*-velocity on a representative *z*-plane ($z = h/2$). As expected, the value of *x*-velocity is intermediate in front of a pin-fin, small behind the pin-fin and large at the two sides. The intersecting boundary-layers of any two adjacent cylinders have been nicely captured in Figure 5a.

The presence of two major components, viz. v_x and v_y results into streamline bending in the proximity of the cylindrical fins. The streamlines on the plane $z = h/2$ are shown in Figure 5b. Figure 5c displays the corresponding pressure distribution revealing the characteristics of the wake regimes. Since L_{Row} is not large, the wake region behind the cylinders of the first row will significantly influence the flow past the second row and this effect will be propagated to further downstream.

It is observed that v_z is the minor component of velocity and its magnitude is one order less than v_y.

In the neighborhood the heat sink, the source of non-zero v_z is firstly due to the temperature difference between the hot base-plate and the cold top wall DCGH of the channel (Figure 3), and secondly, due to the boundary layers adjacent to the bottom and top walls of the channel. Figure 5d shows the contours of *z*-vorticity. The values of *z*-vorticity clearly indicate the clockwise and counter clockwise rotation on the opposite sides of a cylindrical pin fin. The streamline bending can be quantified by the values of *z*-vorticity.

Three dimensional CFD simulations are coordinated over a wide range of Reynolds number $8500 < Re < 36000$. Under forced convective cooling, the role of orientation angle (β)on the performance of the heat sink has been investigated. The non-dimensional surface heat flux, viz. Nusselt number denoted by Nu ($Nu \equiv q_w d_h / k[T_w - (T_{in} + T_{out})/2]$) is evaluated at each $\beta$for various values of Re .In the expression of Nu , T_w is the area averaged temperature of the heated surface and T_{out} is the area averaged temperature of the outlet plane. Both T_w and T_{out} are obtained as output parameters of the present CFD simulations. Figure 6 shows that over a wide range of Re, Nu attains maxima when β equals 120^o.So, the heat transfer for $\beta = 120^o$ is always greater than the heat transfer for $\beta = 0^o$.In this context, it should be mentioned that the previous researchers with the same geometrical model used $\beta = 0^o$.Later we'll investigate the reasons for achieving maxima at $\beta = 120^o$. For the time being, we highlight a few other important observations. Figure 6 displays that for low and intermediate Reynolds number, the minimum Nu appears at $\beta = 90^o$ and 270^o. When Re is large, the minimafor Nu no more occur at $\beta = 90^o$ and 270^o (see the graph corresponding to $Re = 35860$).

For further understanding, we have calculated the maximum, minimum and average temperatures of the heat sink at various β for a fixed Re. The maximum temperature $T_{\max}$ occurs at the lower surface of the base plate; the minimum temperature $T_{\min}$ is found at the fins' top ends; and, the average temperature T_{avg} occurs in between. Figure 7 displays the variation of maximum, minimum and average temperature of the fin-arrayed heat sink with various orientation angle (β). The results are taken with the values of following parameters: $q_w = 5903$ W/m^2 , $T_{in} = 300$ K, $\mathrm{Re} = 9380$ and air as working fluid. It can be observed from Figure 7 that $T_{\max}$ is the minimum when $\beta = 120^o$ and it is the maximum when either $\beta = 90^o$ or $\beta = 270^o$. Therefore, Nu whose value is an indicative of the heat transfer from the base plate, is the maximum when $\beta = 120^o$; and, it is the minimum when $\beta = 90^o$ or $\beta = 270^o$(see Figure 6). Furthermore, both $T_{\min}$ and T_{avg} are found to be the maximum for $\beta = 90^o$ or $\beta = 270^o$(Figure 7). Thus, the heat sink would provide the poorest forced convective cooling when $\beta = 90^o$or $\beta = 270^o$.

It is to be noted that the staggered arrangement is transformed into an inline arrangement for $\beta = 90^o$ or $\beta = 270^o$. Figure 2 indicates that the arrangement corresponding to $\beta = 90^o$ is obtained as a mirror reflection of that corresponding to $\beta = 270^o$. Thus these two arrangements would provide identical results (observed in all the graphs shown in this paper).

External power supply is required to create a pressure difference for constant flow rate of air by overcoming the resistance of the fin-arrayed heat sink. The definition of power coefficient ψ adopted here is the same as Guha and Sengupta (2017) and has been derived from Buckingham Pi Theorem. ψ is the ratio of the fan power input ($\dot{W}$) to a hydrodynamic power quantity ($\rho U_i^3 d_\square^2$), thus, $\psi \equiv \dot{W} / \rho U_i^3 d_\square^2$.Figure 8 displays ψ at various β for a fixed Re .Like other figures here also the same inlet air temperature and the same heat flux at fin base are considered but the Reynolds number is 19290.The power input $\dot{W}$is the product of the average total pressure at the inlet plane and the volume flow rate. It has been found that power requirement varies negligibly with a change in β . Therefore, it can be inferred from Figures 6 and 8 that an increase in heat transfer by rotating the heat sink by 120^o is achieved without any penalty. Thus, a judicial choice of the orientation can be treated an effective method for improving the performance of a fin-arrayed heat sink.

Why, out of all possible values of β , the maximum benefit is realized at 120° remain unanswered. Going to resolve this question, we found that the reasons are twofold. First we would explore the geometric reasons. The projected area of the fin array (in the *x*-direction on to the outlet plane) would be the maximum when β equals $60^\circ, 120^\circ, 240^\circ, 300^\circ$. The ratio of the projected area for $\beta = 120^\circ$ and that for $\beta = 0^\circ$ is 1.45.(The ratio of the projected area corresponding to $\beta = 90^\circ$ and that corresponding to $\beta = 0^\circ$ is 0.57). The through-flow velocity increases with an increase in the projected area. Hence, the greater the projected area the greater would be the heat transfer. Secondly, the positioning of individual fin inside the channel plays an important role. Figure 9 shows the temperature distribution on the surface of fin arrayed heat sink for $\beta = 0^\circ$ and $\beta = 120^\circ$. The figure clearly exhibits that for the case of $\beta = 120^\circ$, more number of fins take part in forced convection more actively.

When β equals 0° the last two rows do not participate so actively as the first two rows do. (Observe the temperature contours from the base plate towards the fins' upper end in Figure 9). On the other hand, for the case of $\beta = 120^\circ$, all fins participate in transferring heat more or less uniformly. The explanation may be as follows. For $\beta = 0^\circ$, the first row fully obstructs the third row and the second row fully obstructs the fourth row; but for $\beta = 120^\circ$ the first row partially obstructs the third row and the second row partially obstructs the fourth row. However, it is to be realized that the geometric explanation alone is not capable of resolving the issue: why the maximum benefit is obtained at $\beta = 120^\circ$. Therefore, next we are taking cue of a thermo fluid dynamic explanation.

When the values of β are 60°, 120°, 240° and 300° the total number of rows is 5 along *x*-direction (see Figure 2). For $\beta = 60^\circ$ and $\beta = 300^\circ$, the number of fins in each row isfollows:1-3-4-4-2.For $\beta = 120^\circ$ and $\beta = 240^\circ$, the number of fins in each row is follows:2-4-4-3-1.For $\beta = 120^\circ$ or $\beta = 240^\circ$, the first 3 rows contain 10 fins whereas for $\beta = 60^\circ$ or $\beta = 300^\circ$ the first 3 rows contain 8 fins. The presence of greater conducting surfaces in the place where the temperature difference between the fluid and the solid is comparatively large yields a greater effectiveness to the cases corresponding to $\beta = 120^\circ$ or $\beta = 240^\circ$.

A greater three-dimensionality of the flow in the vicinity of the fin array would determine a more effective heat transfer. At the inlet, the only non-zero component of velocity is v_x. The other two components of velocity vector, viz. v_y and v_z are evolved due to the presence of the fin array and the walls of the rectangular channel.

It is difficult to exactly measure the strength of three-dimensionality of the flow. Out of three velocity components, the through flow component v_x depends mainly on the projected area of the fin array in the *x*-direction on to the outlet plane.

Since the projected area for $\beta = 120^\circ$ is identical to that for $\beta = 240^\circ$, we therefore focus only on the variations of v_y and v_z across the heat sink. We consider two separate *x*-planes; viz. plane A and plane B. Plane A is located just before the heat sink (at $x = 729.3$ mm) and plane B is located just after the heat sink at (at $x = 870.7$ mm).Mass flow averaged v_y and v_z are calculated on plane A and plane B. Table 2 shows that, as compared to the case of $\beta = 240^\circ$, the orientation $\beta = 120^\circ$ results into greater magnitudes of v_y and v_z on the plane B. A greater three-dimensionality yields good mixing and hence increases the effectiveness of heat transfer.

β	Mass flow averaged v_y at Plane A (mm/s)	Mass flow averaged v_y at Plane B (mm/s)	Difference between Plane A & Plane B (mm/s)	Mass flow averaged v_z at Plane A (mm/s)	Mass flow averaged v_z at Plane B (mm/s)	Difference between Plane A & Plane B (mm/s)
12	-7.2	19.1	26.3	-7.9	2.6	10.5
24	1.3	15.0	13.7	-7.8	1.2	8.9

Table 2 Flow three-dimensionality for $\beta = 120^\circ$ and $\beta = 240^\circ$ ($q_w = 5903$ W/m^2, $T_{in} = 300$ K, Re $= 19290$, and air as working fluid)

IV. CONCLUSION

A computational fluid dynamics (CFD) study is performed to investigate the forced convective cooling of a horizontal heat sink with vertical fin-array.The fins are embedded in a staggered arrangement on the base-plate of the horizontal sink. Present study is coordinated with an aim to reveal the effect of orientation angle (β) on the performance of the heat sink. Simulations are performed over a wide range of inflow Reynolds number (Re).

Thus, the insensitivity of the power coefficient ψ with respect to the orientation angle β and the possibility for obtaining an optimum β, for which Nusselt number (Nu) would be the maximum, are explored here. It has been found that the optimum β hovers around 120° irrespective of the values of Re.

We concluded that three major factors are simultaneously responsible in obtaining the optimum performance at 120°.First of all, for $\beta = 120^\circ$, the projected area of the fin array in

the *x*-direction onto the outlet plane is the maximum. This ensures a greater through-flow velocity resulting into a greater the heat transfer.

Secondly, at this β, the positioning of the fin-array within the channel ensures the presence of greater conducting surfaces in the place where the temperature difference between the fluid and the solid is comparatively large.

Finally, three-dimensionality in the flow through the fin array is evolved most effectively for $\beta = 120^\circ$. A greater three-dimensionality yields good mixing which in turn offers a greater heat transfer.

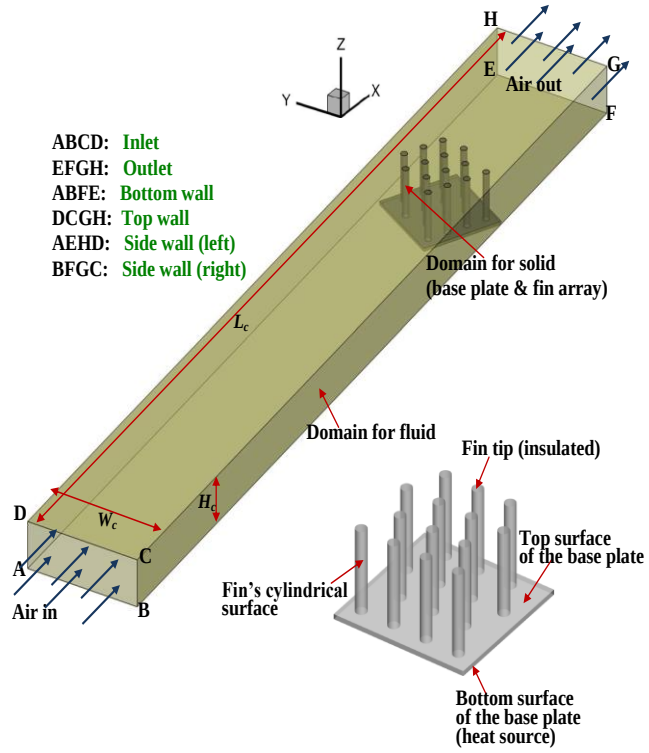

Figure 3 Computational domain and boundary conditions used in the present CFD simulations

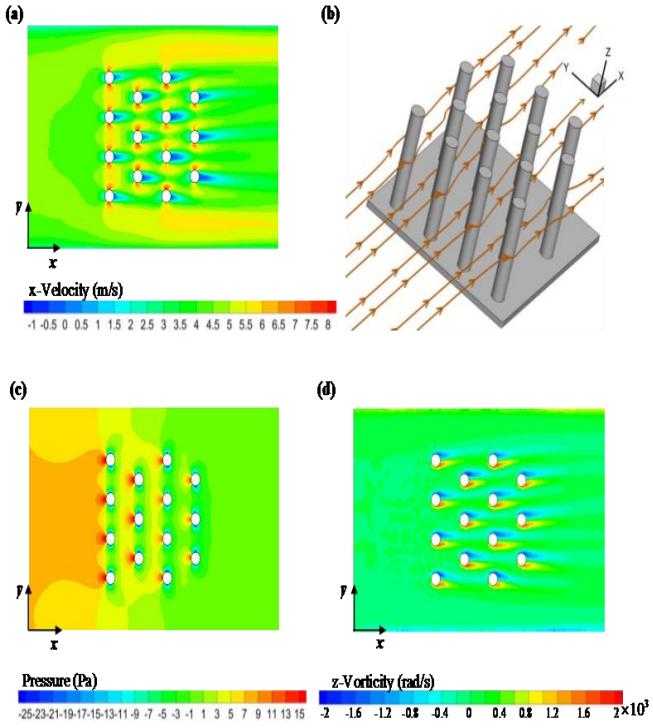

Figure 5. Streamlines and contours pattern: (a) contours of x-velocity on $z = h/2$; (b) streamlines started at $z = h/2$; (c) contours of pressure on $z = h/2$, (d) contours of z-vorticity on $z = h/2$

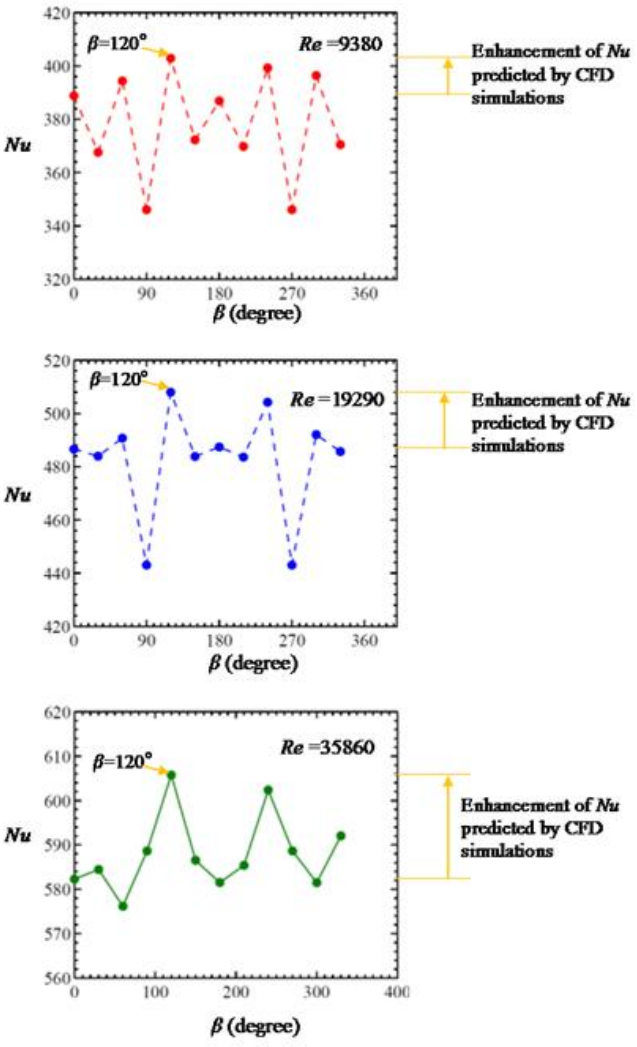

Figure 6 Variation of the Nusselt number (Nu) in one complete revolution of the heat sink about z-axis.

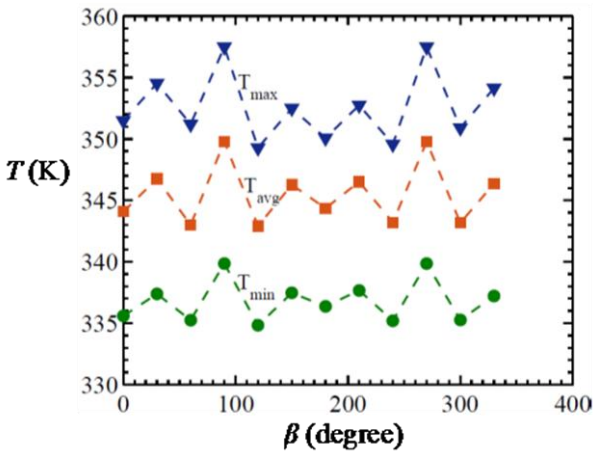

Figure 7 Variation of maximum, minimum and average temperature of the fin-arrayed heat sink with orientation angle (β)

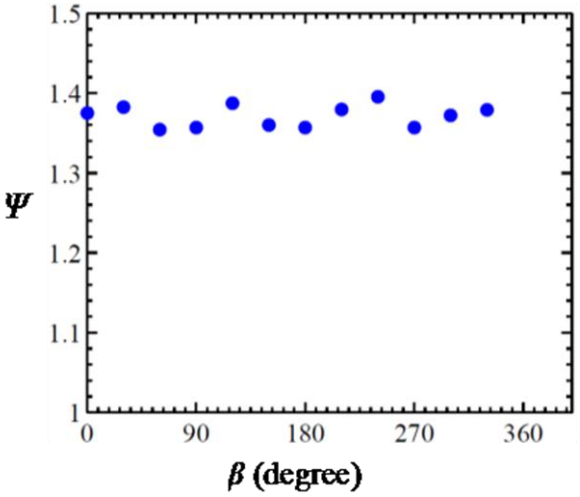

Figure 8 Variation of the power coefficient, ψ $(\equiv \dot{W} / \rho U_i^3 d_h^2)$, in one complete revolution of the heat sink about z-axis

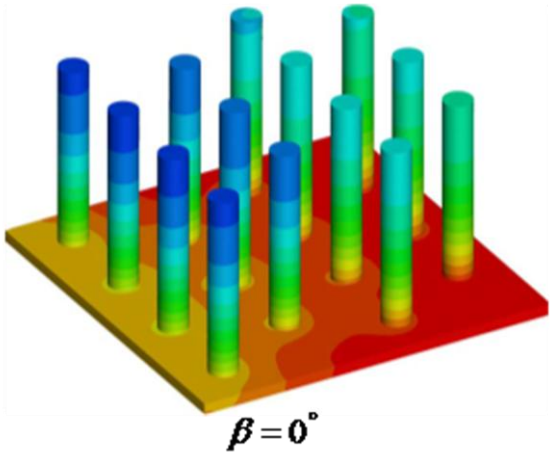

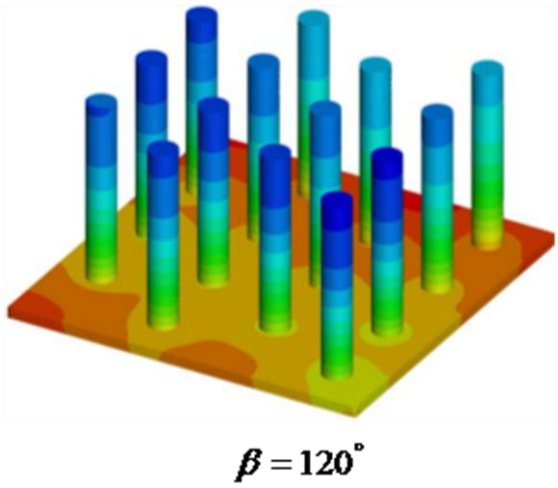

Figure 9 Temperature distributions on the fin-arrayed heat sink [Results correspond to $q_w = 5903$ W/m^2, $T_{in} = 300$ K, Re $= 9380$ and air as working fluid]

REFERENCES

1. Al-Damook, A., Kapur, N., Summers, J. L., and Thompson, H. M. (2015). An experimental and computational investigation of thermal air flows through perforated pin heat sinks. Applied Thermal Engineering, 89, 365–376.
2. Al-Damook, A., Kapur, N., Summers, J. L., and Thompson, H. M. (2016). Computational design and optimisation of pin fin heat sinks with rectangular perforations. Applied Thermal Engineering, 105, 691–703.
3. Bhanja, D., Kundu, B., and Mandal, P. K. (2013). Thermal analysis of porous pin fin used for electronic cooling. Procedia Engineering, 64, 956-965.
4. Burmeister, L. C. (1993). *Convective heat transfer*.John Wiley & Sons.
5. Chin, S. B., Foo, J. J., Lai, Y. L., and Yong, T. K. K. (2013). Forced convective heat transfer enhancement with perforated pin fins. Heat and Mass Transfer, 49(10), 1447-1458.
6. Eckert, E. R., and Drake, R. M. (1972). *Analysis of Heat Transfer*.McGraw-Hill.
7. Elshafei, E. A. M. (2010). Natural convection heat transfer from a heat sink with hollow/perforated circular pin fins. *Energy*, *35*(7), 2870-2877.
8. Fluent 16.0 User's Guide, ANSYS Fluent Inc. (2016), Central Source Park, 10 Cavendish Court, Lebanon, NH 03766, USA.
9. Guha, A., and Sengupta, S. (2017) A non-dimensional study of the flow through co-rotating discs and performance optimization of a Tesla disc turbine. *Proceedings of the Institution of Mechanical Engineers, Part A: Journal of Power and Energy*, 231(8), 721-738.
10. Haley, K. W., and Westwater, J. W. (1966).Boiling heat transfer from single fins.In Proc. Third Intern. Heat Transfer conference, *13*, 245-253.
11. Li, C. H. (1983). Optimum cylindrical pin fin. *AIChE journal*, *29*(6), 1043-1044.
12. Liaw, S. P., Yeh, R. H., and Yeh, W. T. (2005).A simple design of fins for boiling heat transfer. *International journal of heat and mass transfer*, *48*(12), 2493-2502.
13. Lin, Z. M., Wang, L. B., and Zhang, Y. H. (2014). Numerical study on heat transfer enhancement of circular tube bank fin heat exchanger with interrupted annular groove fin. Applied Thermal Engineering, 73, 1465–1476.
14. Maji, A., Bhanja, D., and Patowari, P. K. (2017). Numerical investigation on heat transfer enhancement of heat sink using perforated pin fins with inline and staggered arrangement. Applied Thermal Engineering, 125, 596-616.
15. Patankar, S. V. (1980) *Numerical Heat Transfer and Fluid Flow* Hemisphere, Washington, DC.
16. Razani, A., and Zohoor, H. (1991). Optimum dimensions of convective-radiative spines using a temperature correlated profile. *Journal of the Franklin Institute*, *328*(4), 471-486.
17. Sahin, B., and Demir, A. (2008). Thermal performance analysis and optimum design parameters of heat exchanger having perforated pin fins. *Energy conversion and management*, *49*(6), 1684-1695.
18. Salviano, L. O., Dezan, D. J., and Yanagihara, J. I. (2016). Thermal-hydraulic performance optimization of inline and staggered fin-tube compact heat exchangers applying longitudinal vortex generators. Applied Thermal Engineering, 95, 311–329.
19. Seyf, H. R., and Layeghi, M. (2010). Numerical analysis of convective heat transfer from an elliptic pin fin heat sink with and without metal foam insert. *Journal of Heat Transfer*, *132*(7), 071401.
20. Sonn, A., and Bar-Cohen, A. (1981).Optimum cylindrical pin fin. *Journal of Heat Transfer*, *103*(4), 814-815.
21. Sparrow, E. M., Ramsey, J. W., and Altemani, C. A. C. (1980). Experiments on in-line pin fin arrays and performance comparisons with staggered arrays. *ASME J. Heat Transfer*, *102*(1), 44-50.
22. Vahabzadeh, A., Ganji, D. D., and Abbasi, M. (2015). Analytical investigation of porous pin fins with variable section in fully-wet conditions. *Case Studies in Thermal Engineering*, *5*, 1-12.
23. Yang, A., Chen, L., Xie, Z., Feng, H., and Sun, F. (2016).Constructal heat transfer rate maximization for cylindrical pin-fin heat sinks, Applied Thermal Engineering, 108, 427–435.
24. Yeh, R. H., and Liaw, S. P. (1993).Optimum configuration of a fin for boiling heat transfer. *Journal of the Franklin Institute*, *330*(1), 153-163.

25. Yeh, R. (1997). An analytical study of the optimum dimensions of rectangular fins and cylindrical pin fins. *International journal of heat and mass transfer*, *40*(15), 3607-3615.
26. Yu, X., Feng, J., Feng, Q., and Wang, Q. (2005). Development of a plate-pin fin heat sink and its performance comparisons with a plate fin heat sink. Applied Thermal Engineering, 25(2-3), 173-182.
27. Žukauskas, A. (1972). Heat transfer from tubes in crossflow. *Advances in heat transfer*, *8*, 93-160.
28. Zhao, J., Huang, S., Gong, L., & Huang, Z. (2016). Numerical study and optimizing on micro square pin-fin heat sink for electronic cooling. Applied Thermal Engineering, 93, 1347–1359.

AUTHORS PROFILE

Mr. Pabitra Kumar Mandal, is presently working as an Assistant Professor, Grade-II in the Department of Mechanical Engineering at Dr. B. C. Roy Engineering College, Durgapur, West Bengal, India. He did his B.E. (Mechanical) from Jalpaiguri Government Engineering College under University of North Bengal in the year of 2003. After that he did M. Tech. from I.I.T – Kharagpur in the Department of Aerospace Engineering in the year 2006. His area of expertise includes: Analytical heat transfer, Heat transfer augmentation, Electronic cooling, Heat transfer through porous surface, Solar collector, Renewable energy, Optimization techniques, CFD. He is the life member of Indian Society for Heat and Mass Transfer (Regd.).

Dr. Sayantan Sengupta, is presently working as an Assistant Professor, Grade-I in the Department of Mechanical Engineering in NIT Durgapur, West Bengal. Before that he was in Dr. B. C. Roy Engineering College, Durgapur, West Bengal from August 2017 to October 2018 in Department of Mechanical Engineering. He did his B.E. (Mechanical) from Jalpaiguri Government Engineering College under University of North Bengal in the year of 2009. After that he did M.Tech. from I.I.T – Kharagpur in 2011 and awarded Ph.D. in the year 2017 from same Institute. His area of expertise includes: Analytical heat transfer, Heat transfer augmentation, Electronic cooling, Heat transfer through porous surface, Solar collector, Renewable energy, Optimization techniques, CFD. To date he has published 10 research articles in various SCI/SCIE indexed journals and around 30 papers in various other International journals and conferences.

Dr. Subhas Chandra Rana, is working as an Associate Professor in the Department of Mechanical Engineering at the National Institute of Technology, Durgapur, India. He did his B. Tech. in the Department of Mechanical Engineering from REC Durgapur in the year of 1988 and M.Tech. from same Institute in the year of 2002.He done his Ph.D. from I.I.T- Madras in the year of 2016. He also has long industrial experience of about 13 years at M.A.M.C, Durgapur -713210. His research interests include thermo-acoustic instability, computational fluid dynamics and heat transfer. He had guided Ph.D. scholars and holds publications in reputed journals and conferences.

Dr. Dipankar Bhanja, is presently working as an Assistant Professor, Grade-I in the Department of Mechanical Engineering in NIT Silchar, Assam. Before that he was in Dr. B. C. Roy Engineering College, Durgapur, West Bengal from Aug'04 to Feb '13 and Dumkal Institute of Engineering and Technology, Murshidabad, West Bengal since Feb'02 as a faculty in Department of Mechanical Engineering. He did his B.E. (Mechanical) from Jalpaiguri Government Engineering College under University of North Bengal in the year of 2000. After that he did M.E. from Jadavpur University in 2002. His area of expertise includes: Analytical heat transfer, Heat transfer augmentation, Electronic cooling, Heat transfer through porous surface, Solar collector, Renewable energy, Optimization techniques, CFD.